Grid-Forming Converter DC-link Control considering the Primary Energy Source using a Genetic Algorithm

Carlo De Paolis Robles[a], Andrés Tomás-Martín[a], Ignacio Egido[a], Aurelio García-Cerrada[a]

[a]*Institute for Research in Technology (IIT), Comillas Pontifical University, calle Alberto Aguilera, 23, 28015, Madrid, Spain*

Abstract

The gradual substitution of conventional synchronous generators by electronic generators raises concerns about the reduction of conventional inertia in electric power systems and the ensuing threat to the stability of those systems. In this regard, grid-forming voltage source converters have been proposed as one of the solutions to tackle this problem. Although a growing body of literature addresses DC-link voltage regulation in grid-forming converters, most existing approaches implicitly assume an ideal and unconstrained DC power source. As a result, the dynamic response and operational limits of the primary energy source (PES)—which can critically shape the available DC side power during transients—are rarely modeled or explicitly accounted for in the design of the DC-link control. With a specific control realization, this paper shows that taking those aspects into consideration from the design stage helps to minimize the possibility of a disconnection of the converter from the power grid when a sudden power imbalance occurs while maximizing the resiliency of the system. The paper provides a systematic methodology to adjust the control parameters. The performance of the proposed control is validated by simulation using a commonly accepted detailed model.

Keywords: Grid connectivity, grid-forming, primary energy source, DC-link, genetic algorithm.

Nomenclature

Genetic Algorithm:

Δu_{dc} Incremental error in the DC-link voltage between the setpoint and the actual value

IAE_p Integral of Absolute Error for output power

IAE_{u^2} Integral of Absolute Error for squared DC-voltage

penalty Penalty term added for constraint violation

$e_p(t)$ Instantaneous absolute error in output power

$e_{u^2}(t)$ Instantaneous absolute error in squared DC voltage

J Fitness function score to be minimized

lb Parameter lower bound

p_{load} Load setpoint signal demanded

$p_{\text{out-sp}}$ Setpoint for the converter output power

p_{out} Actual converter output output power

$p_{\text{pes-sp}}$ Setpoint for the Primary Energy Source

p_{pes} Actual Primary Energy Source power

T Simulation time horizon for error integration

$u_{\text{dc-sp}}$ Setpoint DC-link voltage

u_{dc} DC-link voltage

ub Parameter upper bound

w_1 Weighting factor for power error

w_2 Weighting factor for squared DC-link voltage error

1. Introduction

A significant transformation in power systems is underway due to the increased penetration of Renewable Energy Sources (RESs) interfaced through Electronic Power Converters (EPCs) and the retirement of conventional Synchronous Generators (SGs), leading to a marked reduction in rotational inertia [1]. Low-inertia systems exhibit larger frequency excursions after disturbances because physical inertia limits the Rate of Change of Frequency (ROCOF) before primary control reacts [2], and although EPCs can deliver fast frequency support, it remains uncertain whether Fast Frequency Response (FFR) alone can fully compensate for this loss [3]. To address this, the European Network of Transmission System Operators for Electricity (ENTSO-E) proposed in 2023 a set of mitigation measures [4], distinguishing Foundational Measures—which include Voltage Source Converters (VSCs) with Grid-Forming (GFM) capability able to emulate virtual inertia [5]—from Enhanced Response Measures, based on Grid-Following (GFL) converters that provide rapid support but cannot respond instantaneously due to their reliance on the detection of grid voltage [5]. Within this framework, the development and deployment of Grid-Forming Voltage-Source Converters (GFM-VSCs) emerges as a key solution for maintaining adequate frequency stability in future low-inertia systems [6].

Recent studies on frequency stability in converter-dominated systems model the Direct Current link (DC-link) side with varying degrees of detail. Many system-level analyses still assume an ideal DC-link and an instantly available primary energy source, thereby neglecting Direct Current (DC)-side dynamics and limits when studying inertia and ROCOF behaviour [7, 8]. Some even claim that the DC-link has little influence on frequency regulation as long as neither the source nor the converter saturates [9]. By contrast, a growing line of research explicitly accounts for DC-link capacitor dynamics and develops dedicated voltage-control strategies, recognising that robust frequency regulation and transient stability hinge on proper DC-link voltage management.

Some authors study DC-link dynamics from a system-level stability viewpoint, embedding grid-forming converter models with explicit DC-link dynamics in large benchmark networks (e.g., IEEE 9–68 bus test systems) to assess impacts on closed-

loop stability and grid interactions. Reference [10] shows that matching-controlled GFM-VSCs possess inherent DC-link voltage stability under DC-side current saturation, unlike other GFM strategies, extending the framework of [11]. Its follow-up [12] addresses this limitation with a sliding-mode controller that stabilises the DC-link voltage and provides quantifiable FFR, though without ensuring optimality or explicitly handling input constraints. More recently, [13] introduces an Nonlinear Model Predictive Control (NMPC) formulation that incorporates AC/DC current limits and control-input bounds, enabling optimal and tunable FFR. Complementarily, [14] proposes a decentralised nonlinear backstepping controller that regulates the DC-link voltage via active-power adaptation, offering Lyapunov-certified stability with low computational effort. All these references assume a fast Primary Energy Source (PES) represented as an instantaneous current-limited source.

Several authors address DC-side control from a device-level perspective, analyzing how DC-link voltage dynamics couple with grid-forming loops. These works emphasize converter-level modeling and controller design (structure, gains, stability margins, and transients), typically via small-signal/nonlinear analysis and time-domain simulations, and sometimes with laboratory prototype validation. Reference [15] shows how these dynamics influence the transient stability of Virtual Synchronous Generators (VSGs) and classifies DC-link controllers according to the Alternating Current (AC) side variable they modify—either the active-power reference or the internal frequency—while noting that other structures are possible depending on the GFM architecture.

A first group of references regulates the DC-link voltage by adjusting the converter's active power output set point. Reference [16] embeds the DC-link voltage into the synchronisation loop to guarantee regulation while preserving GFM behaviour. Reference [17] places a stronger emphasis on transient stability, proposing a dedicated Proportional-Integral (PI) controller that forces the DC-link capacitor to temporarily absorb power during severe voltage or angle disturbances at the point of connection. This controlled energy absorption effectively reduces the virtual inertia provided by the converter and increases damping, mitigating DC-link overvoltage and increasing the converter transient stability margin. Reference [18] shows that a

PI-based controller acting on the squared voltage may destabilise a droop-controlled GFM inverter during undervoltage events if poorly tuned. All three references use an ideal constant-power PES model any without explicit primary energy source dynamics.

A second group of references regulates the DC-link voltage by adjusting the converter internal frequency. Reference [19] uses a frequency-modulation scheme with a q-axis voltage feedforward (VqFF) loop to add damping and improve voltage regulation. Reference [20] introduces a compensation-based strategy for full-scale Wind Turbine Generators (WTGs), where a lead–lag compensator counteracts the negative damping from large inertia gains, enabling higher inertial coefficients without destabilising the DC-link. In [21], deviations of the squared DC-link voltage directly modulate the internal frequency, allowing inertia emulation without auxiliary storage and preserving GFM behaviour even in weak grids. As in the previous group, these studies assume an instantaneous or constant-power PES, neglecting its dynamics.

Finally, other DC-link control strategies target different variables within the GFM structure. Reference [22] enhances transient stability by acting on the virtual rotor angle inferred from the DC-link dynamics, injecting damping to suppress voltage excursions. Other references regulate the DC-link via a current-controlled ultracapacitor connected through a DC/DC converter. In [23], a cascaded DC-side controller manages the DC-link voltage exclusively through the ultracapacitor branch, with an Energy Management System (EMS) ensuring safe ultracapacitor (UC) operation during active-power support. Reference [24] provides experimental validation of this architecture for inertial response, showing that ultracapacitors can deliver fast frequency support without compromising DC-link stability. These three references model the PES as a constant power injection, without incorporating any dynamic behavior.

Table 1 compiles the most relevant references discussed. For each work, it identifies whether a dedicated DC-link voltage-control strategy is considered and whether this control action coordinates appropriately with a GFM-VSC that provides inertia emulation and Primary Frequency Response (PFR). The table also indicates

whether the proposed control restores the DC-link voltage to its nominal value following a grid-side power disturbance, and it reports the control design methodology adopted in each study. Finally, it clarifies whether upstream PES dynamics on the DC side are modeled and whether the DC-link control explicitly accounts for them to enable grid connectivity while providing frequency support.

Table 1: Comparison of the most relevant references from the Introduction about DC-link methods

Reference	**IE**	**PFR**	**DCNV**	**Design method**	**PESd**	**PESc**
[13]	✓	✓	✓	NMPC	✓*	
[14]	✓	✓	✓	Backstepping	✓*	
[15]	✓	✓	✓	Lyapunov		
[16]	✓	✓		Analytical SG swing eqs.		✓
[17]	✓	✓	✓	Lyapunov		
[18]		✓	✓	Bifurcation-based		
[19]				Small-signal and pole-analysis		
[20]	✓	✓	✓	Three methods†		
[21]	✓	✓	✓	PI-based second-order design		
[22]	✓	✓	✓	Passivity-based / Hamiltonian		
[23]			✓	Cascaded PI		
[24]	✓		✓	Cascaded PI		
This article	✓	✓	✓	Genetic Algorithm (GA)	✓	✓

✓* PES dynamic as a first-order transfer function with 1 ms time constant
† Dynamic DC-link control + damping compensation + lead–lag inertial compensation
IE: Inertia emulation, DCNV: DC-link controlled to nominal value, PESd: Primary Energy Source dynamic consideration, PESc: Primary Energy Source control

The current paper investigates how a GFM-VSC can jointly regulate its DC-link voltage and the power supplied to the grid to remain connected after power disturbances, explicitly modeling PES dynamics rather than assuming an instantaneous or constant-power source. The proposed approach controls both the energy extracted from the PES and the converter active-power output set point similar to [16], which, to the authors' knowledge, is the only existing work that acts on both sides simultaneously. (i) a DC-link voltage control strategy for grid-forming VSCs that provides a fast response to AC-side power imbalances by coordinating the primary energy source and converter power control, thereby enforcing strict DC-link voltage limits and avoiding converter disconnections; and (ii) a GA-based parameter-tuning methodology that optimizes the disturbance step-response performance, first developed on a simplified model and then validated using a detailed Electromagnetic Transient (EMT) model.

The paper is organized as follows. Section 2 describes the nature of the problem in detail and the proposed approach. A design methodology for the DC-link voltage and output control of a GFM-VSC is explained. It also describes the case study to be used in the following sections. Section 3 explains the methodology followed to parameterise the controllers. Section 4 validates the performance of the control in a detailed EMT model of the case study. Section 5 concludes the paper and suggests future work.

2. Description of the problem and case study

To maintain the grid connectivity of the GFM-VSCs, it is critical to coordinate the dynamics of the PES, the AC output power, and the DC-link voltage. This section describes a simplified model developed as a supervisory layer, focusing on the GFM-VSC and PES management time scales.

The case study, illustrated in Figure 1, comprises a PES (representing wind, solar, or Battery Energy Storage System (BESS)), a DC-link capacitor, and a GFM-VSC interface. The AC grid is modeled as an equivalent AC voltage source behind a predominantly inductive grid impedance (Z_{grid}).

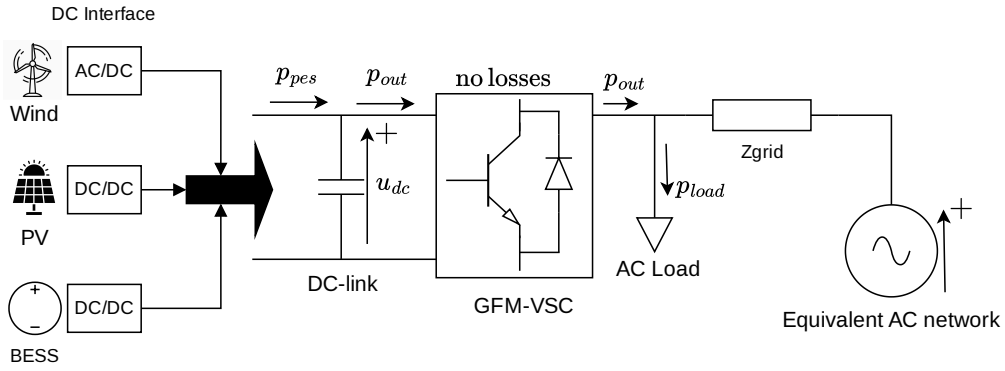

Figure 1: Case study: GFM-VSC with DC-side constraints connected to an AC grid.

2.1. Modelling Hypotheses and System Abstraction

To ensure the tractability of the optimization problem while maintaining physical validity, the following modeling assumptions are adopted:

- **Network and Load Dynamics:** The AC grid is considered static and mainly inductive ($X \gg R$). Under this assumption, the power exchange is governed by the power-angle relationship $P \approx (V_1 V_2/X)\sin(\delta) \approx (V_1 V_2/X)(\delta)$, being δ the angle difference between those two buses. Consequently, any AC load change is observed instantaneously by the converter as a variation in the load angle. An active power change is expected on the event of a frequency deviation (Δf) as per ENTSO-E inertial response validation requirement [25].

- **Converter and GFM Dynamics:** Following the singular perturbation theory [26], the fast internal cascaded control loops and specific GFM implementations (e.g., inertia/damping states, droop couplings, and virtual impedance) are not explicitly represented, given that they are properly designed. Instead, the GFM-VSC is simplified to a first-order transfer function with a time constant $T_c \approx 100$ ms. This abstraction captures the net influence of the AC side on the DC-link power balance through an equivalent mapping from Δu_{dc}^2 to the output converter power set-point.

- **Primary Source Dynamics:** Consistent with the literature presented in the introduction, the PES is modeled as a first-order lag with a time constant T_{PES}, capturing the physical limitations and response delays of the primary energy interface.

- **DC-link Energy Balance:** The DC-link is modeled as a capacitance C. The energy stored, E_{Cap}, is the integral of the power mismatch between the PES (p_{pes}) and the output (p_{out}):

$$E_{Cap}(s) = \frac{1}{s}\left(p_{\mathrm{pes}} - p_{\mathrm{out}}\right) = \frac{1}{2} C u_{dc}^2 \tag{1}$$

  The controls act on u_{dc}^2 as it directly reflects the energy balance of the system.

2.2. Proposed DC-Link Supervisory Control Philosophy

Although the PES-side controller and the converter-side controller, shown in Figure 2, are both driven by the same feedback signal Δu_{dc}^2, their coordination is ensured by a deliberate separation of roles and time scales:

1. **Restoration Loop (*PI-PES*):** This controller handles long-term energy balance, restoring u_{dc} to its nominal value by acting on the PES setpoint, thanks to the Integral part. There is no derivative component in order to avoid excessive setpoit to the PES.
2. **Transient Protection (*PD-out*):** This controller acts on the GFM output power to prevent the voltage from exceeding safety limits $[0.7, 1.15]$ p.u. It is implemented as a Proportional-Derivative (PD) action and intentionally excludes integral action. The proposed control strategy does not affect the steady-state behavior of the GFM-VSC on the AC side, as is normally required for GFM devices. The DC-link control strategy takes over power transients when u_{dc} changes.

This design prevents both loops from simultaneously attempting to remove the same steady-state error in u_{dc}^2, which could otherwise lead to control conflicts and unintended steady-state power redistribution. Consequently, the converter-side loop provides fast transient support to limit DC-link excursions, while the PES-side loop guarantees long-term power balance and recovery, yielding a coordinated response without steady-state interference.

By excluding high-frequency switching and detailed EMT transients, the design process via GA remains computationally efficient. The resulting control set is subsequently assessed in detailed EMT simulations (Section 3), confirming that the proposed DC-link supervisory action remains compatible with realistic AC-side GFM behavior while effectively enforcing DC-link energy limits during severe transients.

3. Control algorithm design methodology

This section covers the control design when using a GA, the formulation of the fitness function used to obtain an effective set of controller parameters. It then provides qualitative remarks to clarify the selection and robustness of the GA hyperparameters, as well as the supervisory nature of the proposed DC-link control. Finally, results are presented, and the logic of abting on both the PES and output converter power is illustrated.

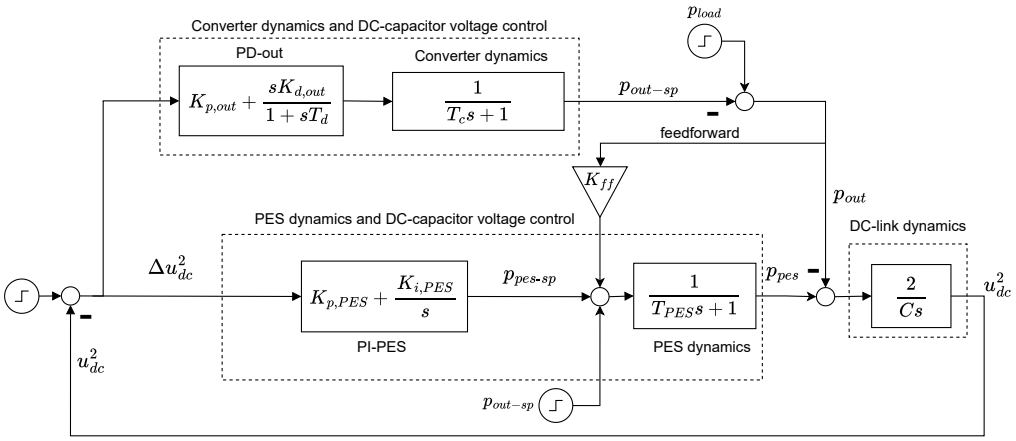

Figure 2: Reduced-order control block diagram representing the supervisory layer and system dynamics.

3.1. Design with a genetic algorithm

The parameters of controllers *PI-PES* and *PD-out* are shown in Figure 2. The design has been carried out with the GA implemented in Matlab, initially introduced in [27], and also explained in reference [28]. GAs are a reliable and effective way to tune controller parameters, as shown in reference [29]. The GA is a method for solving constrained, or unconstrained, optimization problems based on a natural selection process that mimics biological evolution. It iteratively modifies over a population of individual solutions. In each step, the algorithm selects individuals from the current population randomly and uses them as references or parents to produce offspring or descendants for the next generation. Depending on the values given to various parameters, the optimal solution is obtained through the evolution of several or many consecutive generations.

GAs have been widely applied in power and energy systems to optimize controller parameters and improve dynamic performance. For instance, [30] employs a GA to simultaneously tune the Proportional-Integral-Derivative (PID) gains and the fuzzy-logic scaling factors of a Fuzzy–PID controller for an Automatic Voltage Regulator (AVR) system, using a multi-objective function based on Time multiplied Absolute Error (ITAE) and peak output voltage. In [31], an enhanced Maximum Power Point Tracking (MPPT) scheme integrates a GA into the Fractional Open-Circuit-Voltage (FOCV) method to optimally compute the K_v constant under varying irradiance,

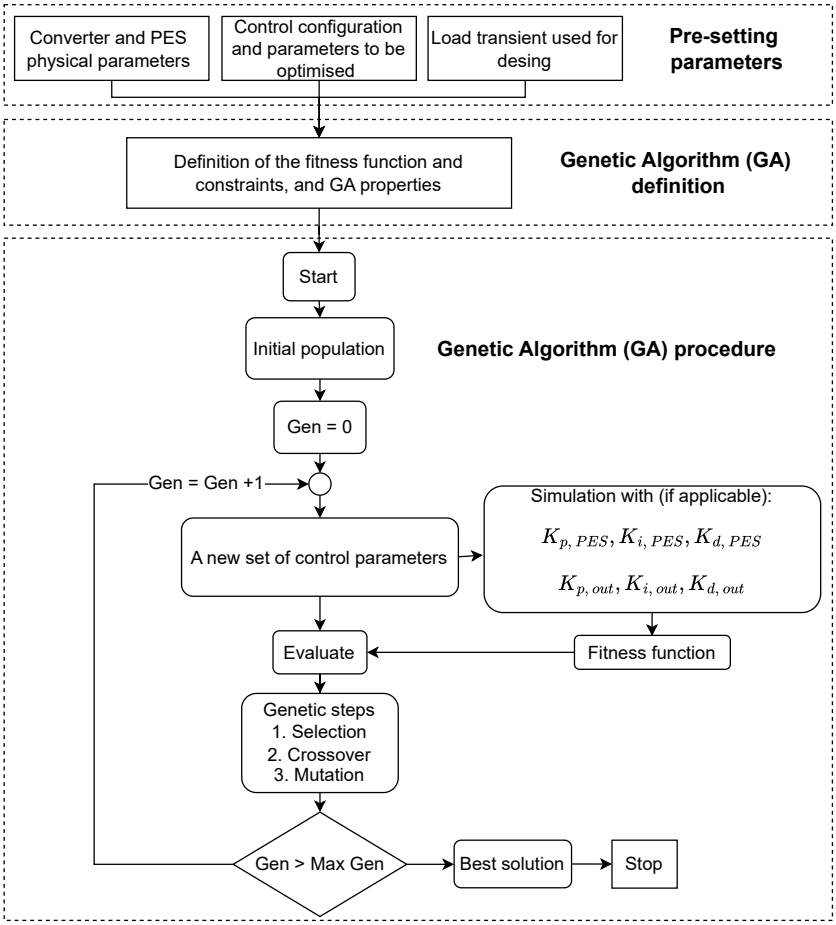

Figure 3: Methodology flow diagram

thereby maximizing Photovoltaic (PV) energy extraction. Likewise, [32] applies a GA to tune the parameters of both a Power System Stabilizers (PSS) and a Static Synchronous Compensators (STATCOM) controller, achieving improved damping and enhanced small-signal stability in a multi-machine power system.

A flow diagram of the methodology used, including the GA, is depicted in Figure 3. It can be described as follows:

1. Depending on the physical characteristics of the converter, PES and the variables to be controlled, the following information must be provided:
   - The pre-fixed physical and grid load parameters:
     - Output power response time of the converter T_c in milliseconds or seconds.

- Capacitance of the DC-link, C, in seconds, following equation (1).
- If a measurement device is available, the selection of including K_{ff} equal to 0 (not chosen or not available) or 1 (chosen or available).
- The PES first-order dynamic time constant, in seconds (T_{PES}).
- The grid Load setpoint that the power converter must withstand, in p.u (p_{Load}).

- The controller parameters to be optimized by the GA, in p.u., are: $K_{p,\,PES}$, $K_{i,\,PES}$, for *PI-PES*, and $K_{p,\,out}$, Kd, *out* for *PD-out*. $K_{d,\,PES}$ and $K_{i,\,out}$ are intentionally set equal to zero. However, they could be included as controller parameters in the optimization, as shown in section 3.4.2, depending on the desired control behavior.
- The fitness function (i.e., the optimization objective) and constraints of the fitness optimization algorithm (see Section 3.2).

2. After defining the pre-settings, the GA properties must be defined in order to start the iterative optimization process.
3. Finally, the GA procedure is executed in order to find the most suitable controller parameters. A detailed description of the genetic algorithm steps can be found in references [29] and [33].

Selecting T_{PES} is a key step in this process. While [34] and [35] indicate that, for technologies such as PV systems and BESSs, the DC-link dynamics may allow energy delivery within approximately 1–10 ms, [36] notes that the practical response time often lies at the upper end of this range or even exceeds it. Moreover, it is not evident that such fast power variations are always desirable. For instance, [37] emphasises that WTGs require limits on the rate of power change to prevent mechanical and electrical stress, even when advanced control strategies are employed to provide FFR, as in [38]. For these reasons, and as summarised in Table 3, we adopt a conservative value of approximately 1 s for T_{PES}.

In addition, it should be noted that a step change in system load, as shown in Figure 2, was selected as the input signal, since any mismatch between generation

and consumption in the grid is perceived by the converter as a load variation. Reference [39] proposes state-space disturbance equations for frequency stability analysis, which clarifies how load step disturbances can be equivalently represented as step disturbances at the terminals of synchronous generators and renewable units.

3.2. Optimization problem, and fitness function used

Controller parameters were calculated by solving the following optimization problem:

$$\min_{p,u^2} \quad J = w_1 \cdot \mathrm{IAE}_p + w_2 \cdot \mathrm{IAE}_{u_2} + \mathrm{penalty} \tag{2}$$

subject to:

Starting from $penalty = 0$, and $\forall\ \mathrm{signal}_i(t) \in \{p_{out\text{-}sp},\ p_{\mathrm{out}},\ p_{\mathrm{pes\text{-}sp}},\ p_{\mathrm{pes}}\}$

$$\text{if } \mathrm{signal}_i(t) > 1, \qquad \mathrm{penalty} += 1000 \cdot \sum \left(s_i(t) - 1\right), \tag{3}$$

$$\text{if } \mathrm{signal}_i(t) < 0, \qquad \mathrm{penalty} += 1000 \cdot \sum \left(-s_i(t)\right), \tag{4}$$

$$\text{if } u^2_{\mathrm{dc}}(t) > (1.15)^2, \qquad \mathrm{penalty} += 1000 \cdot \sum \left(u^2(t) - (1.15)^2\right) \tag{5}$$

$$\text{if } u^2_{\mathrm{dc}}(t) < (0.7)^2, \qquad \mathrm{penalty} += 1000 \cdot \sum \left((0.7)^2 - u^2(t)\right) \tag{6}$$

and,

$$\begin{aligned} &0 \le K_{\mathrm{p,\,PES}} \le 10, \quad 0 \le K_{\mathrm{i,\,PES}} \le 10, \\ &K_{\mathrm{d,\,PES}} = 0, \qquad\quad 0 \le K_{\mathrm{p,\,out}} \le 10, \\ &K_{\mathrm{i,\,out}} = 0, \qquad\quad 0 \le K_{\mathrm{d,\,out}} \le 5 \end{aligned} \tag{7}$$

where $w_1 = 1.0$, $w_2 = 1.0$ and,

$$\mathrm{IAE}_p = \int_0^T e_p(t)\, dt, \quad e_p(t) = |p_{\mathrm{out}}(t) - p_{\mathrm{load}}(t)| \tag{8}$$

$$\mathrm{IAE}_{u^2} = \int_0^T e_{u^2}(t)\, dt, \quad e_{u^2}(t) = \left|u^2_{\mathrm{dc}}(t) - u^2_{\mathrm{dc\text{-}sp}}(t)\right| \tag{9}$$

The formulation above corresponds to an optimization problem with implicit constraints. To ensure constraint satisfaction, a penalty method is employed, i.e., the fitness function includes additive terms that impose high costs when constraints are violated. This penalised fitness function is evaluated for each candidate solution representing a specific set of parameters (chromosome), and a corresponding score is assigned based on performance.

During each generation of the GA, the algorithm evaluates the population and applies selection, crossover, and mutation operators to evolve the solutions to minimise the fitness score (J). The evolutionary process continues iteratively until no significant improvement is detected according to a predefined function tolerance criterion. Parameters $w1$ and $w2$ could be used to prioritise either IAE_p or IAE_{u_2}, if necessary. Equation (8) calculates Integral of Absolute Error (IAE) between p_{out} and the p_{Load}, while (9) calculates the IAE of the u_{dc}^2 and the $u_{\text{dc-sp}}^2$.

Equation (3) limits the maximum value of any signal ($1\,p.u.$, was used) and it is applied to $p_{out\text{-}sp}, p_{\text{out}}, p_{\text{pes-sp}}, p_{\text{pes}}$. Equation (4) limits the minimum value ($0\,p.u.$, was used) for the same signals. A penalty is applied if any of these limits are exceeded. An important condition is that the squared DC-link voltage does not exceed certain limits ($0.7^2 < u_{\text{dc}}^2 < 1.15^2$) to prevent the disconnection of the power converter. Therefore, a high penalty is applied if u_{dc}^2 exceeds those limits as shown in (5) and (6). Finally, (7) gives the lower and upper bounds of the controller parameters selected. $K_{d,\,PES}$ and $K_{i,\,out}$ were left out of the optimization and were given a default value equal to zero ($K_{d,\,PES} = 0$, $K_{i,\,out} = 0$). When $K_{i,\,out} \neq 0$, the final value of $p_{\text{out}} \neq p_{\text{Load}}$ when $u_{\text{dc-sp}}^2$ is driven back to its initial value, due to that in the steady state the converter will not respect the frequency droop imposed on the AC side, which is not the intended response. In addition, $K_{d,\,PES}$ is imposed to be equal to zero, in order to avoid excessive demand on the PES.

This approach allows the GA to explore feasible solutions; however, the qualitative remarks in Section 3.3 are essential for a successful implementation."

3.3. Qualitative remarks about GA characteristics: hyperparameters, optimization search space, robustness and convergence

The GA hyperparameters used in the optimization are summarized in Table 2 and were selected through preliminary trials to obtain reliable and repeatable solutions while keeping the computational burden reasonable. The adopted configuration of GA parameters is sufficiently conservative for the case represented. The relatively large population, the maximum number of generations imposed, and the small percentage of the elite fraction allow for finding a suitable solution in which the variation of controller parameters is almost negligible. This is also obtained thanks to the stall-generation and tolerance-error-based GA parameters.

Table 2: GA parameters applied on the example

GA option	**Selection**
Function tolerance	$1e^{-6}$
Constraint tolerance	$1e^{-3}$
Max. Stall Generation	50
Population Elite Count	5%
Max. number of Generations	200
Population Size	100
Algorithm	Adapatative & feasible
Generation	Deterministic

It must be highlighted that the GA is applied, deliberately, to a limited optimization search space. In this work, only four DC-link control parameters are tuned under constrained bounds. In addition, as explained in Section 2, we are not optimizing the hypothesis applied for a complete set of GFM-VSC parameters. We are not claiming to obtain a globally optimal parameter set, but rather to find a suitable and effective parameter set for the DC-link control, assuming the aforementioned hypothesis.

Another characteristic to note is that the resulting parameter set depends on the operation point. The obtained set of parameter gains depends on the active-power operating point, the available power reserve of the PES, the DC-link capacitance, and the DC-link control bounds. Consequently, this strategy does not allow for finding a global optimal solution independent of the operation point. If those conditions change significantly, the parameters should be re-optimized.

Consequently, considering the set of GA hyperparameters, DC-link control parameter bounds, and the operation point, premature convergence was not observed. However, premature convergence is a possible outcome, as in some situations the accumulated error is so high that no suitable solution can be found. If this happens, it could be mitigated by tightening the GA configuration (e.g., increasing population size and/or maximum generations, and reducing tolerances), performing multi-start runs with different random initial populations, and restarting the search while keeping the best solution found so far, at the cost of additional computation and assuming that the final solution is feasible for the analyzed operating point.

3.4. Results

This section presents the results obtained using the GA. A base case with a representative 0.1 p.u. load increase is first reported, followed by an illustration of the rationale for coordinating the PES power and the converter output power in response to DC-link deviations.

3.4.1. Base Case

This section reports the response of the GA-tuned control to a 0.1 p.u. increase in AC-side active-power demand. The values of the predefined parameters and the optimized controller gains are shown in Table 3. Table 2 shows the GA parameters and options selected, besides the default ones from MATLAB. T_{PES} and T_c are considered to be considerably slow, with respect to the values found in the literature (e.g., in reference [16]). In addition, the equivalent capacitance corresponds to approximately 1.3 mF (derived from a time constant of 0.02 s) when expressed in Farads, for a power converter rated at 15 kVA and 680 V in DC, similar to the converter used in [40]. This value is comparable to the 1 mF capacitor employed on the DC side in that reference. The conversion between the capacitance expressed in seconds and in Farads is obtained using equation (10), which is derived from equation (9) in [41]:

$$\mathrm{E}_{stored} = S_N(W) * C(s) = \frac{1}{2} * C(F) * U_{dc}^2(V) \tag{10}$$

where E_{stored} is the total energy stored in the capacitor, S_N is the nominal converter power in watts, $C(s)$ is the equivalent DC-link capacitance expressed in seconds, $C(F)$ is the capacitance in Farads, and U_{dc} is the nominal DC voltage.

Figure 4 shows the evolution of the parameters involved in the optimization process as the GA progresses. Clearly, from approximately generation 150 onward, the controller parameters change little.

Figure 5 shows the first two seconds of a simulation run with the simplified model after a 0.1 p.u. stepwise increment in the AC load takes place. The steady-state time is marked with a dashed vertical line when u_{dc}^2, p_{out}, and p_{pes} reach 99% of their final values (also their setpoint values). As there is no much energy stored in the DC-link capacitor, the voltage initially decays to $0.91 p.u.$, approximately (see the upper subplot). It then quickly recovers to $0.99 p.u.$ in about 0.60 seconds. The fast recovery is due to *PD-out* (which acts on the output power of the converter). Eventually, it settles to $u_{\mathrm{dc\text{-}sp}}^2$, thanks to the *PI-PES* controller.

The lower subplot of Figure 5 shows p_{out} and p_{pes} of the converter. Firstly, the converter tries to deliver the power that is demanded from the grid. However, as the DC-link voltage rapidly decays, the power converter quickly reduces its output power down to $\approx 0.48 p.u.$. Once the DC-link recovers, the output power stabilises at $\approx 0.59 p.u.$, in around ≈ 0.55 seconds.

3.4.2. Logic behind acting on both the PES and the output of the power converter

The rationale for coordinating the PES power and the converter output power is presented for the same disturbance considered in Section 3.4.1. The benefits of the control acting on both the PES and the output of the power converter can be appreciated in Figure 6 where three cases of parameter fit are compared: (a) GA Best Case: the one in Figure 5; (b) *PID-out*: with only the PID of the converter output power; and (c) *PID-PES*: with only PID of the PES. Note that in this section, for cases (b) and (c), the three variables of the *PID* are optimized through the GA, with respect to case (a), where we set some variables to zero.

In the case *PID-out*, the response against the power disturbance is very fast ($\approx 300ms$), and the restoration of u_{dc}^2 is basically instantaneous. However, the

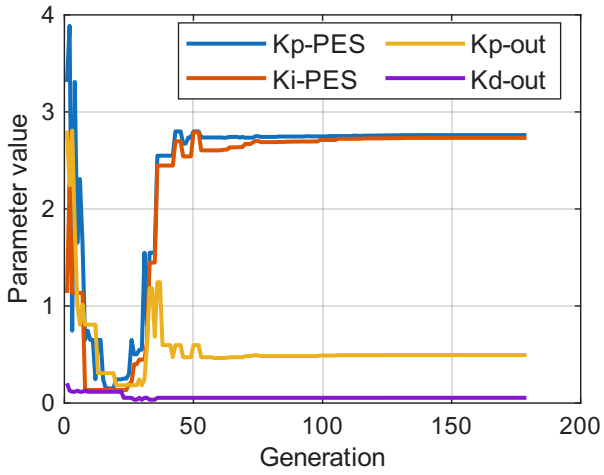

Figure 4: Evolution of controller parameters during the GA optimization

obtained power response is not satisfactory, as the analysis aims to capture the steady-state primary frequency response, which depends on the PES. Since the PES remains inactive, its output power is unchanged, leaving the inertial response determined only by the limited energy stored in the DC-link capacitor. As a result, the converter output power fails to track the grid's power step in steady state. The integral component of the PID controller ensures that the initial reference setpoint is followed, thereby restoring u_{dc} to its nominal value.

Meanwhile, in the case where only the *PID-PES* is used, the GA cannot find an appropriate parametrisation in order to comply with the constraints. The restoration of the u_{dc}^2 is very slow, and it almost exceeds both the maximum and minimum thresholds. In addition, the converter output power seems to reach instantaneously the power requested from the grid. However, this is only achieved by exceeding the maximum limit of the power extracted from the PES, which is not a realistic response.

The results in the example demonstrate that the proposed methodology, acting upon the PES and the converter output power simultaneously, to control the DC-link voltage, is clearly beneficial.

4. Detailed model simulation validation

This section validates the proposed DC-link control using an EMT model. In the EMT model, we simulate the control response and compare it with that of the

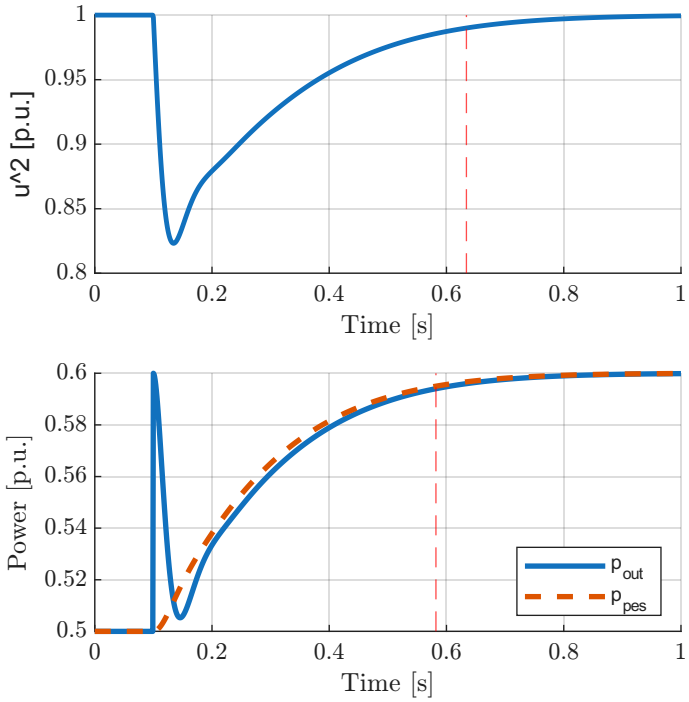

Figure 5: Control response of u_{dc}^2, p_{out} and p_{pes}

Table 3: Parameters applied on the simplified case

Parameters		
C (s)=0.02	$u_{\text{dc-sp}}^2 = 1$	$p_{\text{out-sp}}$ (p.u.) $= 0.5$
$p_{\text{load-ini}}$ (p.u.) $= 0.5$	$p_{\text{load-fin}}$ (p.u.) $= 0.6$	T_{PES} (s) $= 1$
T_{c} (s) $= 0.1$	$K_{\text{ff}} = 0$	
$K_{\text{p, PES}}$ (p.u.) $= 2.7614$	$K_{\text{i, PES}}$ (p.u.) $= 2.7324$	$K_{\text{d, PES}}$ (p.u.) $= 0$
$K_{\text{p, out}}$ (p.u.) $= 0.4944$	$K_{\text{i, out}}$ (p.u.) $= 0$	$K_{\text{d, out}}$ (p.u.) $= 0.0540$

simplified model, replicating the study presented in Section 3.4.1.

This model is implemented using the tool described in reference [42].The models implemented in this tool have been previously tested in the laboratories of the Energy Madrid Institute for Advanced Studies (IMDEA). It has also been cross-checked against Simscape Electrical models, as described in [42].

Figure 7 depicts the case system for the validation of the results in a detailed model. It is composed of two GFM-VSC connected through a line, and a load connected at each line end. The following assumptions are considered:

- GFM-VSC$_1$ has a PES and output power converter dynamics associated, as in the model in Section 3. The values of the parameters are the same as indicated in Table 3. Both simplified and detailed models will be simulated in order to

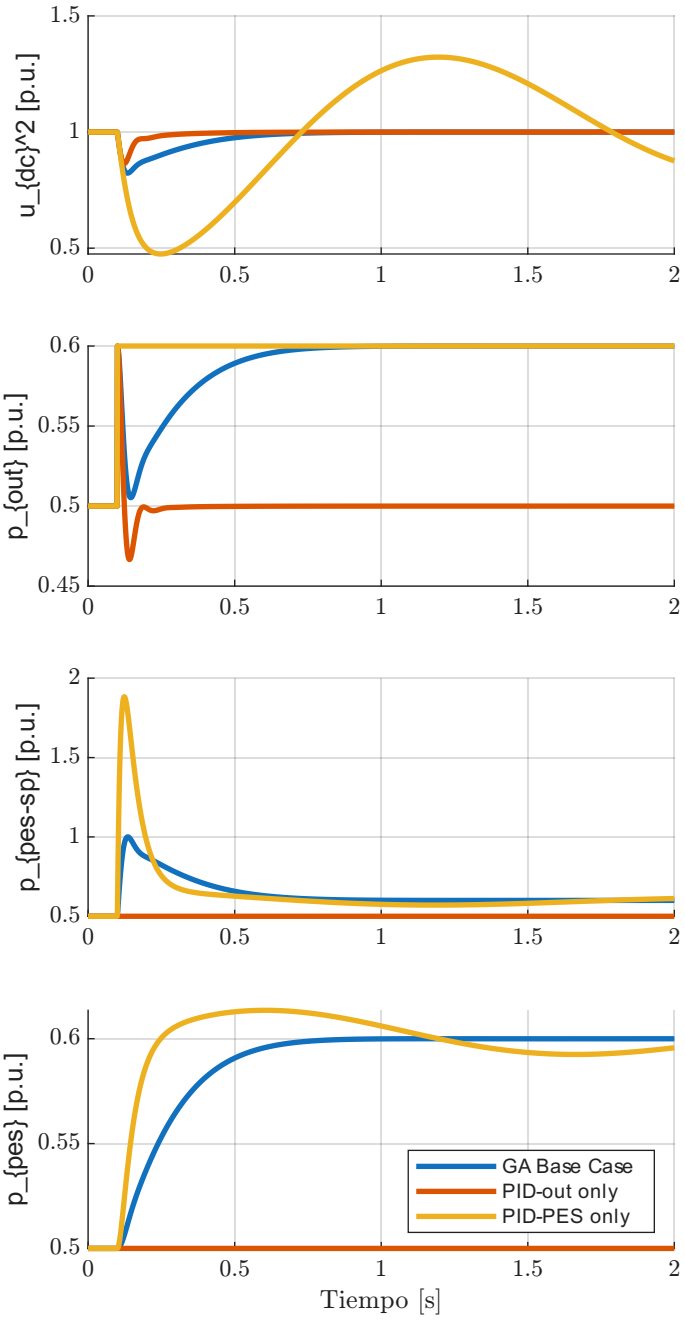

Figure 6: Control response of u_{dc}^2 and p_{out}

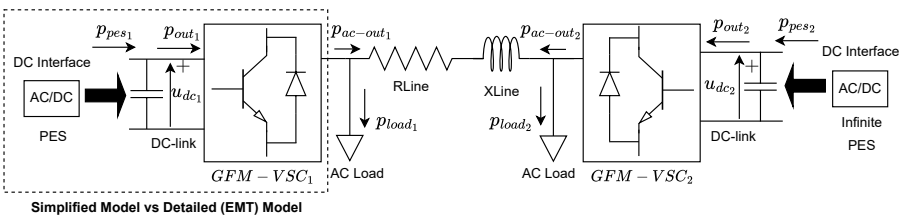

Figure 7: Case study of the detailed model system: two GFM-VSCs interconnected

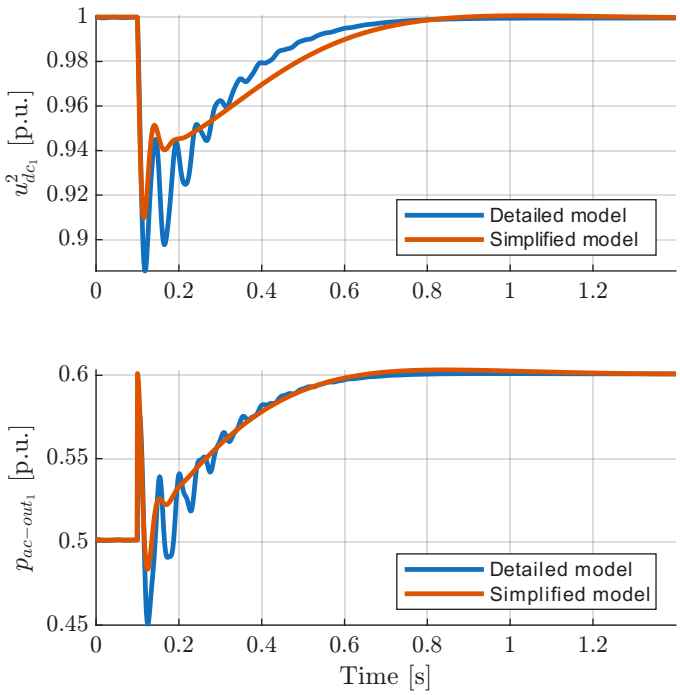

Figure 8: Control response comparison between models

compare the response of the control implemented.

- GFM-VSC$_2$ has a PES with infinite and instantaneous power provision, and no DC dynamics.
- Each GFM-VSC is initially delivering 0.5 p.u. Each load consumes 0.5 p.u.
- A 0.1 p.u. step increase in both loads (AC Load 1 for the simplified and the EMT models) at t = 0.1 seconds is simulated.

The first subplot in Figure 8 shows the u^2_{dc} response of the GFM-VSC$_1$ in both the simplified and detailed models. The second subplot in Figure 8 shows the p_{out} response of the GFM-VSC$_1$ in both the simplified and detailed models. As represented in both figures, the results obtained with the simplified and the detailed models match well. It demonstrates that the model proposed to design the DC-link control is adequate, and it confirms the validity of the results.

5. Conclusions and future work

This article proposes a DC-link supervisory control strategy for GFM-VSCs, together with a methodology to tune its parameters, that coordinates both the con-

verter output power and (when available) the PES reserve power. The control is optimized to prevent converter disconnection by keeping the DC-link voltage within admissible limits while coordinating accordingly with a GFM-VSC that provides inertial and primary-frequency support. The optimization objective explicitly accounts for both DC-link voltage excursions and converter output-power tracking. The proposed DC-link control layer is first designed using a simplified model and then validated in a detailed EMT model. The results show that the achievable output GFM-VSC power response is strongly influenced by the mismatch between PES power provision and the available DC-link capacitance. Future work will focus on establishing an equivalence between inertia provided by GFM-VSCs and that of SGs, to support a secure transition toward RES-dominated power systems.

Acknowledgments

This work is part of the Project PID2021-125628OB-C21 funded by MICIU/AEI-/10.13039/501100011033.

References

[1] M. N. H. Shazon, A. Jawad *et al.*, "Frequency control challenges and potential countermeasures in future low-inertia power systems: A review," *Energy Reports*, vol. 8, pp. 6191–6219, 2022.

[2] S. Saha, M. Saleem, and T. Roy, "Impact of high penetration of renewable energy sources on grid frequency behaviour," *International Journal of Electrical Power & Energy Systems*, vol. 145, p. 108701, 2023.

[3] F. Dörfler and D. Groß, "Control of low-inertia power systems," *Annual Review of Control, Robotics, and Autonomous Systems*, vol. 6, no. 1, pp. 415–445, 2023.

[4] ENTSO-E, "Project Inertia - Phase II: Updated Frequency Stability Analysis in Long Term Scenarios, Relevant Solutions and Mitigation Measures," ENTSO-E, Rue de Spa, 8, 1000 Brussels, Belgium, Tech. Rep., 2023.

[5] Y. Li, Y. Gu, and T. C. Green, "Revisiting grid-forming and grid-following inverters: A duality theory," *IEEE Transactions on Power Systems*, vol. 37, no. 6, pp. 4541–4554, 2022.

[6] H. Zhang, W. Xiang, W. Lin, and J. Wen, "Grid forming converters in renewable energy sources dominated power grid: Control strategy, stability, application, and challenges," *Journal of modern power systems and clean energy*, vol. 9, no. 6, pp. 1239–1256, 2021.

[7] Z. I. Mahmood, H. Cui, B. She, and F. F. Li, "Evaluating the equivalent inertia of grid-following and grid-forming inverter-based resources," *IEEE Transactions on Energy Conversion*, 2024.

[8] E. A. Ducoin, Y. Gu, B. Chaudhuri, and T. C. Green, "Analytical design of contributions of grid-forming and grid-following inverters to frequency stability," *IEEE Transactions on Power Systems*, vol. 39, no. 5, pp. 6345–6358, 2024.

[9] R. W. Kenyon, A. Sajadi, M. Bossart, A. Hoke, and B.-M. Hodge, "Interactive power to frequency dynamics between grid-forming inverters and synchronous generators in power electronics-dominated power systems," *IEEE Systems Journal*, vol. 17, no. 3, pp. 3456–3467, 2023.

[10] S. Samanta and N. R. Chaudhuri, "Stability analysis of grid-forming converters under dc-side current limitation in primary frequency response regime," *IEEE Transactions on Power Systems*, vol. 37, no. 4, pp. 3077–3091, 2021.

[11] A. Tayyebi, D. Groß, A. Anta, F. Kupzog, and F. Dörfler, "Frequency stability of synchronous machines and grid-forming power converters," *IEEE Journal of Emerging and Selected Topics in Power Electronics*, vol. 8, no. 2, pp. 1004–1018, 2020.

[12] S. Samanta, N. R. Chaudhuri, and C. M. Lagoa, "Fast frequency support from grid-forming converters under dc-and ac-side current limits," *IEEE Transactions on Power Systems*, vol. 38, no. 4, pp. 3528–3542, 2022.

[13] S. Samanta, C. M. Lagoa, and N. R. Chaudhuri, "Nonlinear model predictive control for droop-based grid forming converters providing fast frequency support," *IEEE Transactions on Power Delivery*, vol. 39, no. 2, pp. 790–800, 2023.

[14] L. Karunaratne, N. R. Chaudhuri, A. Yogarathnam, and M. Yue, "Nonlinear backstepping control of grid-forming converters in presence of grid-following converters and synchronous generators," *IEEE Transactions on Power Systems*, vol. 39, no. 1, pp. 1948–1964, 2023.

[15] C. Shen, W. Gu, W. Sheng, and K. Liu, "Transient stability analysis and design of vsgs with different dc-link voltage controllers," *CSEE Journal of Power and Energy Systems*, vol. 10, no. 2, pp. 593–604, 2023.

[16] J. Girona-Badia, V. A. Lacerda, D. W. Spier, E. Prieto-Araujo, and O. Gomis-Bellmunt, "Resource-aware grid-forming synchronization control: Design, analysis and validation," *IEEE Transactions on Energy Conversion*, 2024.

[17] C. Xu, Z. Zou, X. Liu, M. Huang, W. Chen, and Z. Wang, "Stability analysis and control design of grid-forming converters with dc-link effect," *IEEE Transactions on Power Electronics*, 2025.

[18] C. Luo, T. Liu, X. Wang, and X. Ma, "Design-oriented analysis of dc-link voltage control for transient stability of grid-forming inverters," *IEEE Transactions on Industrial Electronics*, vol. 71, no. 4, pp. 3698–3707, 2023.

[19] L. Zhao, Z. Jin, and X. Wang, "Small-signal synchronization stability of grid-forming converters with regulated dc-link dynamics," *IEEE Transactions on Industrial Electronics*, vol. 70, no. 12, pp. 12 399–12 409, 2023.

[20] Y. Qin, H. Wang, D. Zhou, Z. Deng, J. Zhang, and X. Cai, "A novel dc-link voltage synchronous control with enhanced inertial capability for full-scale power conversion wind turbine generators," *IET Renewable Power Generation*, vol. 18, no. 4, pp. 690–705, 2024.

[21] A. Tian, Y. Wu, Z. Hu, Z. Wang, T. Wu, J. Jiang, and Z. Peng, "Two-stage pv grid-connected control strategy based on adaptive virtual inertia and damping control for dc-link capacitor dynamics self-synchronization," *Journal of Energy Storage*, vol. 72, p. 108659, 2023.

[22] Y. Peng, Z. Shuai, C. Shen, X. Hou, and Z. J. Shen, "Transient stabilization control of electric synchronous machine for preventing the collapse of dc-link voltage," *IEEE Transactions on Smart Grid*, vol. 14, no. 1, pp. 82–93, 2022.

[23] A. M. Gross, K.-N. Malamaki, M. Barragán-Villarejo, G. C. Kryonidis, F. J. Matas-Díaz, S. I. Gkavanoudis, J. M. Mauricio, J. M. Maza-Ortega, and C. S. Demoulias, "Energy management in converter-interfaced renewable energy sources through ultracapacitors for provision of ancillary services," *Sustainable Energy, Grids and Networks*, vol. 32, p. 100911, 2022.

[24] G. C. Kryonidis, J. M. Mauricio, K.-N. D. Malamaki, M. Barragán-Villarejo, F. de Paula García-López, F. J. Matas-Diaz, J. M. Maza-Ortega, and C. S. Demoulias, "Use of ultracapacitor for provision of inertial response in virtual synchronous generator: Design and experimental validation," *Electric Power Systems Research*, vol. 223, p. 109607, 2023.

[25] ENTSO-E, "Entso-e publishes phase ii technical report on grid forming requirements," ENTSO-E News, Nov. 2025, last accessed: 2025-12-18. [Online]. Available: https://www.entsoe.eu/news/2025/11/04/entso-e-publishes-phase-ii-technical-report-on-grid-forming-requirements/

[26] L. Rouco, F. Pagola, G. C. Verghese, and I. J. Pérez-Arriaga, "Selective modal analysis," in *Power system coherency and model reduction*. Springer, 2013, pp. 199–258.

[27] J. H. Holland, "Outline for a logical theory of adaptive systems," *Journal of the ACM (JACM)*, vol. 9, no. 3, pp. 297–314, 1962.

[28] "Genetic Algorithm," https://www.mathworks.com/discovery/genetic-algorithm.html.

[29] S. B. Joseph, E. G. Dada, A. Abidemi, D. O. Oyewola, and B. M. Khammas, "Metaheuristic algorithms for pid controller parameters tuning: Review, approaches and open problems," *Heliyon*, vol. 8, no. 5, 2022.

[30] T. Dogruer and M. S. Can, "Design and robustness analysis of fuzzy pid controller for automatic voltage regulator system using genetic algorithm," *Transactions of the Institute of Measurement and Control*, vol. 44, no. 9, pp. 1862–1873, 2022.

[31] A. Hassan, O. Bass, and M. A. Masoum, "An improved genetic algorithm based fractional open circuit voltage mppt for solar pv systems," *Energy Reports*, vol. 9, pp. 1535–1548, 2023.

[32] J. Bhukya and V. Mahajan, "Parameter tuning of pss and statcom controllers using genetic algorithm for improvement of small-signal and transient stability of power systems with wind power," *International Transactions on Electrical Energy Systems*, vol. 31, no. 7, p. e12912, 2021.

[33] B. Alhijawi and A. Awajan, "Genetic algorithms: Theory, genetic operators, solutions, and applications," *Evolutionary Intelligence*, vol. 17, no. 3, pp. 1245–1256, 2024.

[34] B. Pawar, E. I. Batzelis, S. Chakrabarti, and B. C. Pal, "Grid-forming control for solar pv systems with power reserves," *IEEE Transactions on Sustainable Energy*, vol. 12, no. 4, pp. 1947–1959, 2021.

[35] M. Guan, "Scheduled power control and autonomous energy control of grid-connected energy storage system (ess) with virtual synchronous generator and primary frequency regulation capabilities," *IEEE transactions on power systems*, vol. 37, no. 2, pp. 942–954, 2021.

[36] W. Zhou, C. Li, L. Yang, Z. Li, C. Zhang, and T. Zheng, "Analysis of primary frequency regulation characteristics of pv power plant considering communication delay," *Energy Reports*, vol. 9, pp. 1315–1325, 2023.

[37] C. Zhang, J. Li, S. Liu, P. Hu, J. Feng, H. Ren, R. Zhang, and J. Jia, "Coordinated frequency modulation control strategy of wind power and energy storage considering mechanical load optimization," *Energies*, vol. 17, no. 13, p. 3198, 2024.

[38] X. Lyu and D. Groß, "Grid forming fast frequency response for pmsg-based wind turbines," *IEEE Transactions on Sustainable Energy*, vol. 15, no. 1, pp. 23–38, 2023.

[39] R. Gao and H. Wang, "Iterative optimization method for frequency stability constraints in renewable energy-integrated power systems," *IET Generation, Transmission & Distribution*, vol. 19, no. 1, p. e70165, 2025.

[40] F. Göthner, J. Roldán-Pérez, R. E. Torres-Olguin, and O.-M. Midtgård, "Harmonic virtual impedance design for optimal management of power quality in microgrids," *IEEE Transactions on Power Electronics*, vol. 36, no. 9, pp. 10 114–10 126, 2021.

[41] R. Yang, G. Shi, C. Zhang, G. Li, and X. Cai, "Internal energy based grid-forming control for mmc-hvdc systems with wind farm integration," *IEEE Transactions on Industry Applications*, vol. 59, no. 1, pp. 503–512, 2022.

[42] A. Tomás-Martín, C. D. Zuluaga-Ríos, J. Suárez-Porras, J. García-Aguilar, L. Sigrist, A. García-Cerrada, and B. Kazemtabrizi, "A vector-based flexible-complexity tool for simulation and small-signal analysis of hybrid ac/dc power systems," *Sustainable Energy, Grids and Networks*, p. 101817, 2025.